J. Appl. Comput. Mech., 5(2) (2019) 390-401
DOI: 10.22055/jacm.2018.26307.1322

ISSN: 2383-4536
jacm.scu.ac.ir

M&MoCS

Shahid Chamran University of Ahvaz

Journal of Applied and Computational Mechanics

Research Paper

Effect of Exponentially Variable Viscosity and Permeability on Blasius Flow of Carreau Nano Fluid over an Electromagnetic Plate through a Porous Medium

A.K. Abdul Hakeem[1], M.K. Nayak[2], O.D. Makinde[3]

[1] Department of Mathematics, Sri Ramakrishna Mission Vidyalaya College of Arts and Science, Coimbatore - 641020, India

[2] Department of Physics, Radhakrishna Institute of Technology and Engineering, Biju Patnaik University of Technology, Odisha, India

[3] Faculty of Military Science, Stellenbosch University, Private Bag X2, Saldanha 7395, South Africa

Received June 21 2018; Revised October 07 2018; Accepted for publication October 08 2018.
Corresponding author: M.K. Nayak, manoj.nayak@riteindia.in

Abstract. The present investigation draws scholars' attention to the effect of exponential variable viscosity modeled by Vogel and variable permeability on stagnation point flow of Carreau Nanofluid over an electromagnetic plate through a porous medium. Brownian motion and thermophoretic diffusion mechanism are taken into consideration. An efficient fourth-order RK method along with shooting technique are implemented to obtain the required solution of the non-dimensional modeled equations. The contribution of the present study is that augmented electromagnetic field strength due to the suitable arrangement of the plate and that of porosity parameter yield an accelerated motion while that of viscosity parameter produces retarded motion of shear-thickening fluid, contrary to shear-thinning fluid. At the same time, it discusses the inclusion of porous matrix which controls the thermal as well as concentration boundary layers, while enhanced Brownian motion exhibits diametrically opposite trend for them in response to shear-thickening fluid.

Keywords: Vogel's viscosity model, Variable Permeability, Blasius flow, Carreau Nanofluid, Electromagnetic plate.

1. Introduction

In a reasonably attractive looking, power manufacturing, transportation, chemical production, microelectronics, and high-energy devices involved in modern industrial fields received rising demands in the case of effective cooling techniques. Traditional fluids such as water, kerosene, engine oil, and ethylene glycol due to their abysmal low thermal conductivities are unable to be utilized to meet the above cooling techniques. On the other hand, the thermal conductivities of metals, oxides, carbides or carbon nanotubes, and nanowires are extremely higher compared to those of traditional base fluids. In the case of tremendous cooling, novel-type fluids which are called Nano fluids were developed (Choi [1], Xuan and Li [2], and Kumar and Sonawane [3]), which are the mixture of nanoparticles (nanometer-sized particles) with significant heat exchange performance and base fluids. Therefore, Nano fluids have the great advantage of enhanced thermal conductivity compared to the base fluids. Apart from this, the enhancement of heat transfer characteristics of nanofluids was accomplished due to heat transfer mechanisms such as Brownian motion and thermophoresis. With the help of such mechanisms and such effects, boundary layer flow and heat transfer of different Nano fluids flowing past several surfaces have been studied by various researchers (Khan and Pop [4], Hosseinzadeh et al. [5], Ghadikolaei et al. [6-8], Dogonchi et al. [9], Nayak [10], and Nayak et al. [11-12]).

As known, Carreau fluid is a generalized Newtonian fluid which exhibits shear-thinning and shear-thickening behavior. Khan and Azam [13] investigated the heat and mass transfer characteristics of Carreau Nanofluid flow subjected to transverse

Published online: March 22 2019

magnetic field. Furthermore, Khan et al. [14] discussed the time-varying Falkner-Skan flow of Carreau Nanofluid past a wedge where they observed that enhancing the Brownian motion and thermophoretic force upsurges the fluid temperature.

An electromagnetic plate is an arrangement of span-wise aligned array of alternating electrodes and permanent magnets which is fixed on a plane surface. The electromagnetic field due to such arrangement develops an exponentially decaying surface-parallel Lorentz force. Such electromagnetic body force controls the flow separation and eliminates the turbulent effects appearing in the flow. Pantokratoras and Magyari [15] were the pioneers to study electro-magnetohydrodynamic flow over a horizontal Riga plate. The buoyancy effect on the flow of nanofluid over a vertical Riga plate was analyzed by Ahmad et al. [16]. In their study, they have declared that thermal and solutal buoyancy forces enhance the fluid. Nayak et al. [17] have investigated the flow behavior of NaCl-CNP Nano fluid in association with homogeneous and heterogeneous reactions past a vertical Riga plate. Related works on the Riga plates are investigated by many Authors (Mehmood et al. [18], Nayak et al. [19-22]).

It is known to us that regarding the introduction of porous matrix, it provides thermal insulation and promotes heat transfer. The relevance of porous media with boundary layer flow can be perceived from their inevitable applications in the cooling procedure of the nuclear reactors, oil production, electronic cooling systems, heat exchangers, geothermal engineering, and underground disposal of nuclear waste. Roy et al. [23] studied the heat flow visualization in mixed convection inside a porous triangular cavity. Further, Javed et al. [24] pointed out that an increase in Darcy number yields diminution in the heat transfer rate from the top wall while the reverse effect is attained along the bottom wall of the trapezoidal cavities subjected to a magnetic field. Nayak [25] also revealed the influence of porous matrix on chemically reactive magnetohydrodynamic viscoelastic fluid flow past stretched sheet. Recently, Ghadikolaei et al. [26] investigated the flow analysis and radiative heat transfer of Fe_3O_4–$(CH_2OH)_2$ Nano fluid and dusty fluid in a porous medium.

Recently, Ahmad et al. [27] studied the flow behavior of Nano fluid over a Riga plate. However, there are some limitations in their study. Considering such limitations and the relevance of Carreau Nano fluid, stagnation point flow, electromagnetic plate, influence of variable viscosity, and porous matrix, authors motivated to investigate the related aspects. In other words, the objective of the present study is to focus on the effect of exponentially variable viscosity and exponentially variable permeability on Blasius flow of Carreau Nano fluid over an electromagnetic plate implementing Brownian motion and thermophoretic diffusion mechanisms. The previous study by Ahmad et al. [27] lacks focus on some aspects which are incorporated as the novelties of the present study.

The novelties of the current study compared to Ahmad et al. [27] include:

- Carreau Nano fluid is introduced.
- Exponentially variable viscosity modeled by Vogel is considered.
- Exponentially variable permeability is implemented.
- Stagnation point flow is taken into account.
- Brownian motion and thermophoretic diffusion mechanisms are taken into consideration.

2. Formulation of the problem

We consider the steady incompressible stagnation point flow of Carreau Nano fluid over a vertical electromagnetic plate embedded in a porous medium. Effect of exponential variable viscosity associated with Vogel's model is considered. A non-uniform permeability is also taken into account. A Cartesian coordinate system is considered where the x-axis is along the plate and the y-axis is normal to it (Fig.1). Electromagnetic field of the plate induces an exponentially decaying Lorentz force parallel to the plate surface.

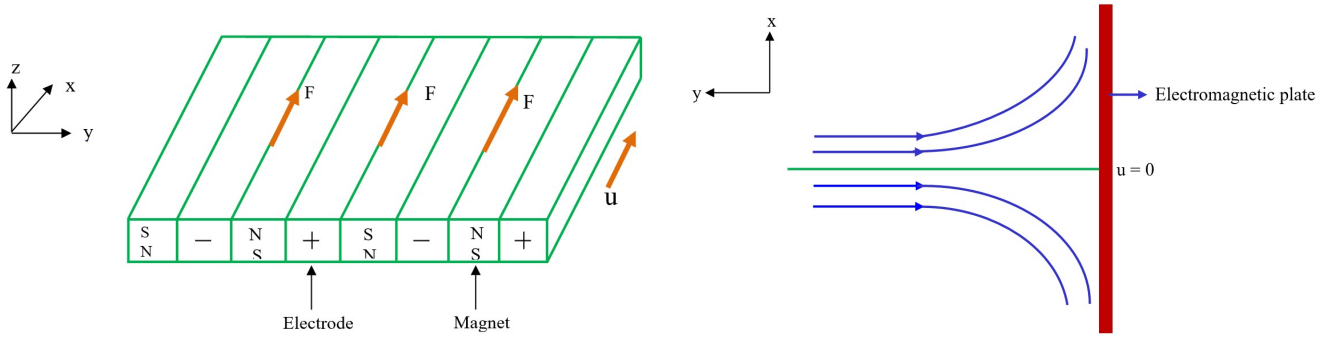

(a) (b)

Fig. 1. Geometry of the problem.

The continuity, momentum, energy, and concentration equations governing the stagnation point of Carreau Nano fluid flow with double stratification and variable viscosity are (Ahmad et al. [27], Alizadeh et al. [28], Dogonchi et al. [29], Ghadikolaei et al. [26, 30] and Hatami et al. [31]):

$$\frac{\partial u}{\partial x}+\frac{\partial v}{\partial y}=0 \tag{1}$$

$$u\frac{\partial u}{\partial x}+v\frac{\partial u}{\partial y}=U_\infty\frac{dU_\infty}{dx}+\frac{1}{\rho_f}\frac{\partial}{\partial y}\left(\mu_f\frac{\partial u}{\partial y}\right)\left[1+\Omega^2\left(\frac{\partial u}{\partial y}\right)^2\right]^{\frac{p-1}{2}}$$
$$+(p-1)\Omega^2\frac{1}{\rho_f}\frac{\partial}{\partial y}\left(\mu_f\frac{\partial u}{\partial y}\right)\left(\frac{\partial u}{\partial y}\right)^2\left[1+\Omega^2\left(\frac{\partial u}{\partial y}\right)^2\right]^{\frac{p-3}{2}}+\frac{\pi j_0 M_0}{8\rho_f}e^{-(\pi/\varepsilon)y}+\frac{\mu_f}{\rho_f}\frac{(U_\infty-u)}{K^*(x)} \tag{2}$$

$$u\frac{\partial T}{\partial x}+v\frac{\partial T}{\partial y}=\alpha_f\frac{\partial^2 T}{\partial y^2}+\tau\left[D_B\frac{\partial C}{\partial y}\frac{\partial T}{\partial y}+\frac{D_T}{T_\infty}\left(\frac{\partial T}{\partial y}\right)^2\right] \tag{3}$$

$$u\frac{\partial C}{\partial x}+v\frac{\partial C}{\partial y}=D_B\frac{\partial^2 C}{\partial y^2}+\frac{D_T}{T_\infty}\frac{\partial^2 T}{\partial y^2} \tag{4}$$

The requisite boundary conditions are (Ahmad et al. [27], Alizadeh et al. [28]):

$$\left.\begin{aligned} u=v=0,\ T=T_w,\ C=C_w \quad at \quad y=0 \\ u=U_\infty=ae^{\frac{x}{L}},\quad T\to T_\infty,\quad C\to C_\infty \qquad as \quad y\to\infty \end{aligned}\right\} \tag{5}$$

where

$$\left.\begin{aligned} T_w=T_\infty+T_0e^{\frac{x}{2L}},\ C_w=C_\infty+C_0e^{\frac{x}{2L}} \\ K^*(x)=K_0e^{-\frac{x}{L}} \end{aligned}\right\} \tag{6}$$

here Ω is the time material parameter, p is the power-law index. $\alpha_f=k_f/(\rho C_p)_f$ is the thermal diffusivity, and $\tau=(\rho C_p)_p/(\rho C)_{pf}$ is the heat capacity ratio. Also, D_B is the Brownian diffusion coefficient and D_T is the thermophoretic diffusion coefficient. $U_\infty(x)=ae^{x/L}$ is the free stream velocity of the Riga plate, $K^*(x)$ is the exponentially varying permeability of the medium, K_0 is the constant which contributes to the initial permeability. L is the reference length. λ_0 stands for a constant. Vogel's model accounts for temperature-dependent viscosity. In this model, the expression for temperature-dependent viscosity is as

$$\mu(\theta)=\mu_1e^{-\theta_0}e^{\frac{D}{B_1+\theta}}=\mu_0e^{\frac{D}{B_1+\theta}} \tag{7}$$

where D and B_1 indicate viscosity parameters associated with Vogel's model and $\mu_0=\mu_1e^{-\theta}$ (constant viscosity), respectively. The suitable transformations employed for the purpose are (Ahmad et al. [27], Alizadeh et al. [28]):

$$\left.\begin{aligned} \eta=y\sqrt{\frac{a}{2L\upsilon_f}}\,e^{\frac{x}{2L}},\ \psi(x,y)=\sqrt{2aL\upsilon_f}\,e^{\frac{x}{2L}}f(\eta) \\ \theta(\eta)=\frac{T-T_\infty}{T_w-T_\infty},\ \phi(\eta)=\frac{C-C_\infty}{C_w-C_\infty} \end{aligned}\right\} \tag{8}$$

Now the stream function in (8) is defined as

$$u=\frac{\partial\psi}{\partial y}\qquad\text{and}\qquad v=-\frac{\partial\psi}{\partial x} \tag{9}$$

So Eq. (1) is automatically satisfied. With the help of Eqs. (7) and (8), Eqs. (2), (3), (4) and (5) take the form as:

$$e^{\frac{D}{B_1+\theta}}\left[f'''-\left(\frac{D}{B_1+\theta}\right)^2f''\right]\left\{\left[1+We^2(f'')^2\right]^{\frac{p-1}{2}}\right.$$
$$\left.+(p-1)^2We^2(f'')^2\left[1+We^2(f'')^2\right]^{\frac{p-3}{2}}\right\}-2(f')^2+ff''+2Ze^{-\Lambda\eta}+Ke^{\frac{D}{B_1+\theta}}(1-f')=0 \tag{10}$$

$$\theta''(0)+\Pr\left[f\theta'+Nb\,\theta'\phi'+Nt(\theta')^2\right]=0 \tag{11}$$

$$\phi''+\left(\frac{Nt}{Nb}\right)\theta''+Sc\,f\,\phi'=0 \tag{12}$$

$$\left.\begin{array}{l} f'=0, f=0, \theta=1, \phi=1 \quad at \ \eta=0 \\ f'=1, \theta\to 0, \phi\to 0 \quad as \ \eta\to\infty \end{array}\right\} \tag{13}$$

with

$$\left.\begin{array}{l} Z=\dfrac{\pi j_0 M_0 L}{8\rho_f U_\infty^2}, We=\sqrt{\dfrac{\Omega^2 U_\infty^3}{2L\upsilon_f}}, \Lambda=\dfrac{\pi}{\delta}\sqrt{\dfrac{2L\upsilon_f}{U_\infty}}, K=\dfrac{2L\upsilon_f}{aK_0}, \upsilon_f=\dfrac{\mu_0}{\rho_f} \\ P_r=\dfrac{\upsilon_f}{\alpha_f}, N_b=\dfrac{\tau D_B\left(C_w-C_\infty\right)}{\upsilon_f}, N_t=\dfrac{\tau D_T\left(T_w-T_\infty\right)}{\upsilon_f T_\infty}, Sc=\dfrac{\upsilon_f}{D_B} \end{array}\right\} \tag{14}$$

where Z refers to the modified Hartman number, We is the Weissenberg number, and Λ is the width parameter. Additionally, K stands for the porosity parameter, υ_f is the kinematic viscosity, P_r is the Prandtl number, and N_t is the thermophoresis parameter. In that regard, N_b is the Brownian motion parameter, and *Sc* is the Schmidt number. The local skin friction coefficient C_{fx} is expressed as

$$C_{fx}=\frac{\tau_w\left(x\right)}{\rho_f U_\infty^2\left(x\right)} \tag{15}$$

where $\tau_w\left(x\right)$ denotes the wall shear stress. The non-dimensional local skin friction coefficient can be presented as

$$\sqrt{\frac{2L}{x}}\,\mathrm{Re}_x^{1/2} C_{fx}=e^{\frac{D}{B_1+\theta}}\left[1+We^2\left\{f''(0)\right\}^2\right]^{\frac{p+1}{2}} f''(0) \tag{16-a}$$

The local Nusselt number is expressed as

$$Nu_x=\frac{x\,q_w}{k_f\left(T_f-T_\infty\right)} \tag{16-b}$$

where $q_w=-k_f\left(\partial T/\partial y\right)\big|_{y=0}$ denotes the wall heat flux. The non-dimensional local Nusselt number can be developed as

$$\sqrt{\frac{2L}{x}}\,Re_x^{-1/2} Nu_x=-\theta'(0) \tag{17}$$

The local Sherwood number is expressed as

$$Sh_x=\frac{x\,J_m}{D_B\left(C_w-C_\infty\right)} \tag{18}$$

where $J_m=-D_B\left(\partial C/\partial y\right)\big|_{y=0}$ denotes the wall mass flux. The non-dimensional local Sherwood number can be developed as

$$\sqrt{\frac{2L}{x}}\,Re_x^{-1/2} Sh_x=-\phi'(0) \tag{19}$$

where $\mathrm{Re}_x=xU_\infty\left(x\right)/\upsilon_f$ is the local Reynolds number.

3. Results and Discussion

The present study contributes to the exploration of the Blasius flow of Carreau Nano fluid over an electromagnetic plate through a porous medium which is subjected to Brownian motion and thermophoretic diffusion. What is most interesting in the present study is that the effects of exponential variable viscosity and variable permeability have been analyzed. The solution of the transformed and modeled equations are devised by implementing fourth-order RK method. The current work has presented graphical as well as theoretical analysis involving the characteristic properties of various pertinent physical parameters in response to the fluid velocity, temperature, and concentration in a well-appreciated manner.

Figs. 2-4 impart a realistic analysis about the variation of fluid velocity, temperature, and concentration in response to the different values of viscosity parameter, D, respectively. It is observed that increasing the values of D decelerate the fluid velocity while it yields opposite behavior for fluid temperature and concentration. This stems from the fact that the viscous force overrides the inertial force. As a result, the fluid friction due to this issue restrains the fluid motion. Such a restrained fluid motion enhances the temperature and concentration. This flow, heat, and mass transfer behavior contribute descending velocity boundary layer and ascending thermal boundary layer as well as concentration boundary layer. Further, from Figs. 5-7 it is visualized that the viscosity parameter B_1 creates an accelerated motion (Fig.5). The accelerated motion is envisaged due to the presence of B_1 in the denominator of momentum equation (10). However, opposite behavior is marked in the case of

temperature and concentration in response to an increase in B_1 (Figs. 6 and 7). It is envisioned that the rate of fluid acceleration is low in response to greater B_1. Meanwhile, there is a slow rate of diminishing temperature and concentration in response to a greater B_1 in the entire flow domain.

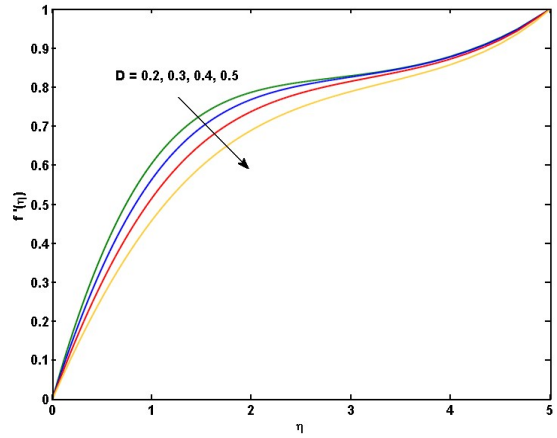

Fig. 2. Effect of D on $f'(\eta)$ for $Z = \Lambda = 0.2, We = 3, K = 0.3, B_1 = 0.5, p = 1.5$

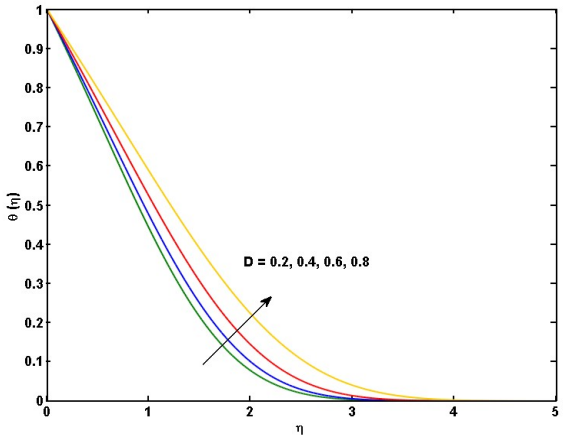

Fig. 3. Effect of D on $\theta(\eta)$ for $Z = \Lambda = 0.2$ $B_1 = 0.5,\ K = 0.3, We = 3, p = 1.5\ , N_b = N_t = 0.2, \Pr = 1.9$

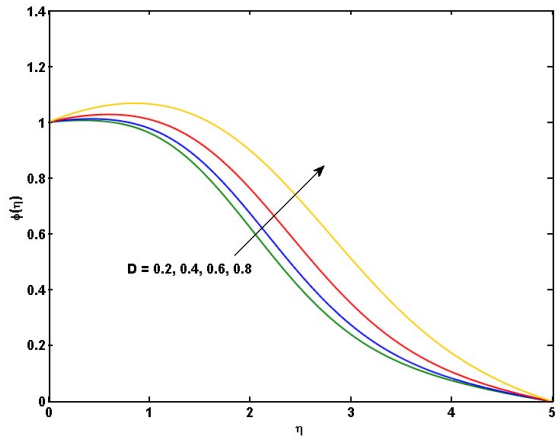

Fig. 4. Effect of D on $\phi(\eta)$ for $Z = \Lambda = 0.2,$ $p = 1.5, We = 3, B_1 = 0.5, K = 0.3, N_b = N_t = 0.2, \Pr = 1.9$

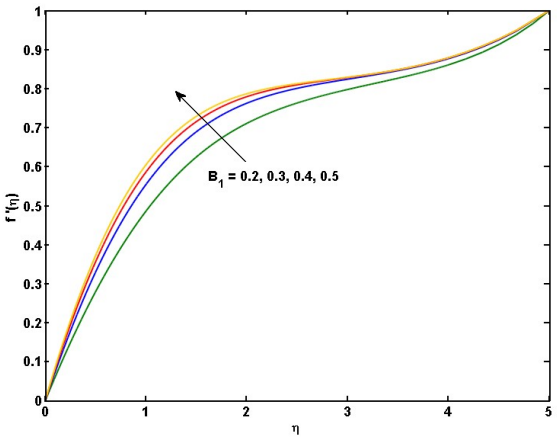

Fig. 5. Effect of B_1 on $f'(\eta)$ for $Z = \Lambda = 0.2,$ $We = 3, K = 0.3, D = 0.2, p = 1.5$

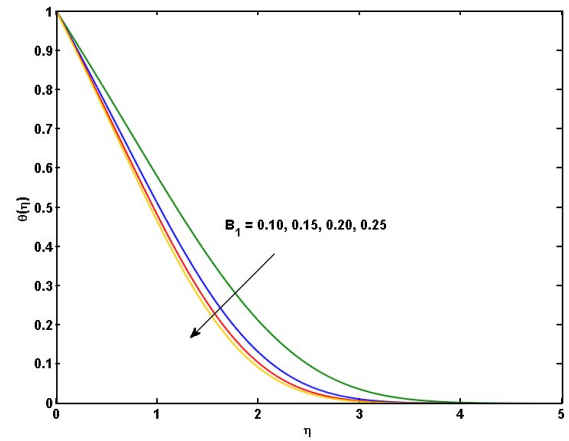

Fig. 6. Effect of B_1 on $\theta(\eta)$ for $Z = \Lambda = 0.2,$ $D = 0.2,\ K = 0.3, We = 3, p = 1.5\ , N_b = N_t = 0.2, \Pr = 1.9$

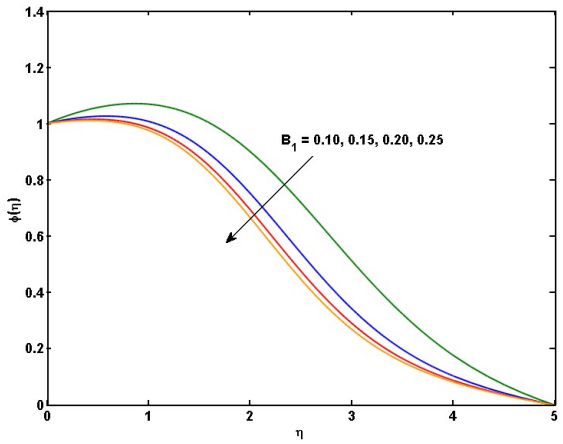

Fig.7. Effect of B_1 on $\phi(\eta)$ for $Z = \Lambda = 0.2,$ $p = 1.5, We = 3, D = 0.2, K = 0.3\ , N_b = N_t = 0.2, \Pr = 1.9, Sc = 1$

An understanding of the effect of We on the velocity, temperature and concentration profiles can be known from Figs. 8, 9, and 10. From the figures, it is clear that increasing values of We supports the generation of accelerated fluid motion. As a result, while those decline the fluid temperature as well as concentration from plate region to ambient fluid in case of shear thickening fluid. It is also seen that MBL is an increasing function of We and thermal boundary layer and concentration

boundary layer are decreasing function of We in shear-thickening fluid. In fact, Weissenberg number is an inverse relation to the fluid viscosity for a specific time material parameter. So, with larger We the thickness of the fluid gets reduced which in turn enhances the velocity. Thus, it undermines the temperature as well as concentration of fluid.

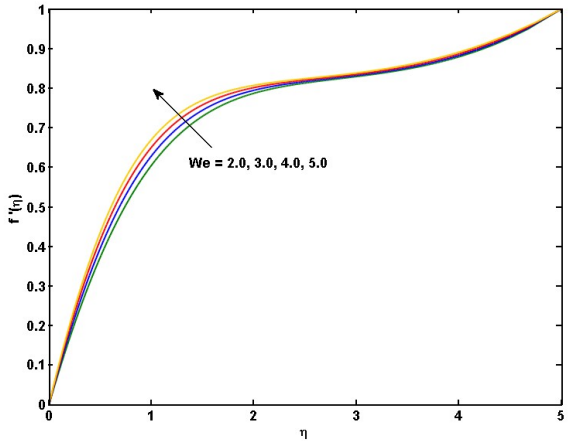

Fig. 8. Effect of We on $f'(\eta)$ for $Z = \Lambda = 0.2$, $B_1 = 0.5, K = 0.3, D = 0.2, p = 1.5$

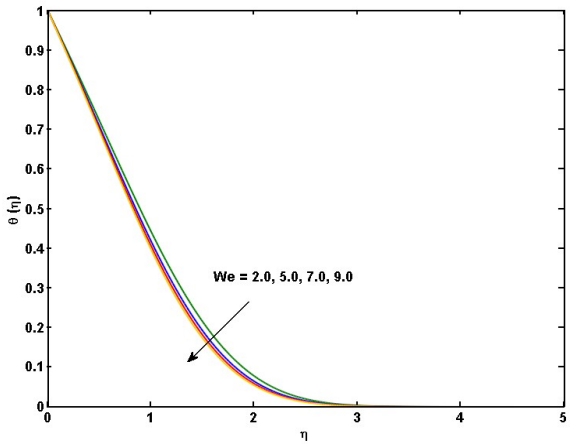

Fig. 9. Effect of We on $\theta(\eta)$ for $Z = \Lambda = 0.2$, $D = 0.2,\ K = 0.3, B_1 = 0.5, p = 1.5\ , N_b = N_t = 0.2, \Pr = 1.9$

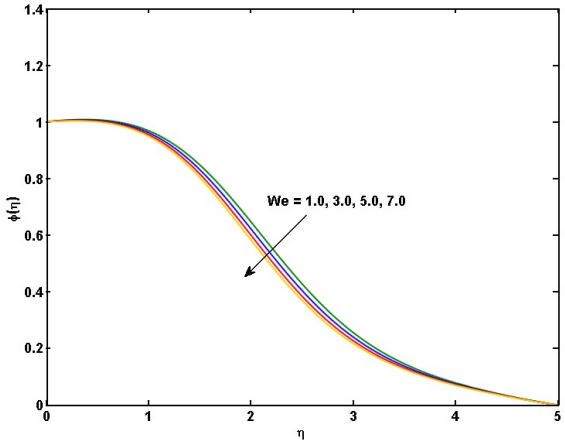

Fig. 10. Effect of We on $\phi(\eta)$ for $Z = \Lambda = 0.2, p = 1.5, B_1 = 0.5, D = 0.2, K = 0.3\ , N_b = N_t = 0.2, \Pr = 1.9, Sc = 1$

The flow, heat and mass transfer behavior of shear-thinning and shear-thickenning liquids are observed in Figs. 11, 12 and 13. An increase in power-law index p upsurges $f'(\eta)$. More elaborately, for shear-thickenning liquids $(p = 1.5, 2.0, 3.0)$, increase rate of fluid velocity is significant compared to that of shear-thinning fluid $(p = 0.5)$. Temperature and concentration decline slowly for shear-thinning liquid $(p = 0.5)$, and faster in shear-thickenning fluid $(p = 1.5, 2.0, 3.0)$.

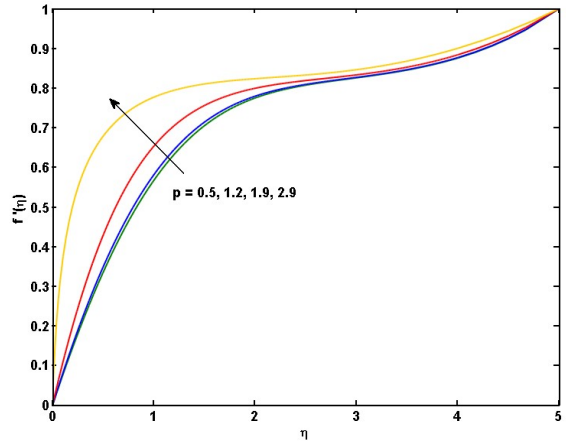

Fig. 11. Effect of p on $f'(\eta)$ for $Z = \Lambda = 0.2$, $B_1 = 0.5, K = 0.3, D = 0.2, We = 3$

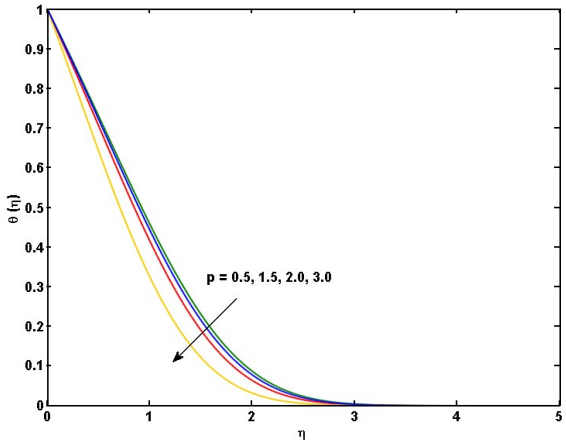

Fig. 12. Effect of p on $\theta(\eta)$ for $Z = \Lambda = 0.2$, $D = 0.2,\ K = 0.3, We = 3, B_1 = 0.5\ , N_b = N_t = 0.2, \Pr = 1.9$

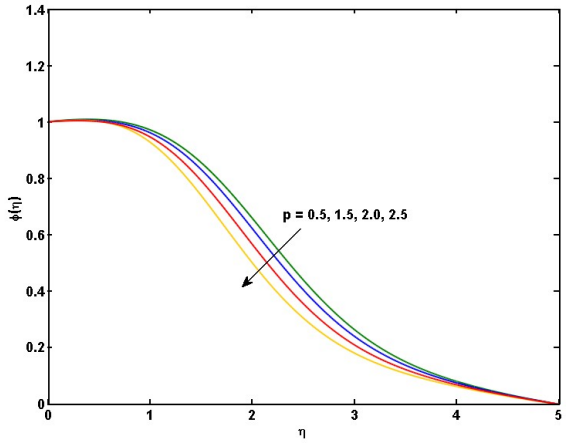

Fig. 13. Effect of p on $\phi(\eta)$ for $Z=\Lambda=0.2$, $We=3, B_1=0.5, D=0.2, K=0.3$, $N_b=N_t=0.2, \Pr=1.9, Sc=1$

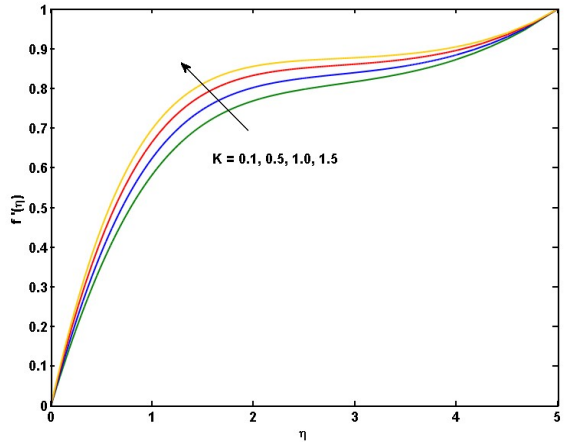

Fig. 14. Effect of K on $f'(\eta)$ for $Z=\Lambda=0.2$, $B_1=0.5$, $D=0.2, We=3, p=1.5$

The influence of porous matrix on velocity, temperature and concentration distributionis are noticed from Figs. 14, 15, and 16 respectively. An increase in permeability parameter, K, enhances the flow velocity while that of K exhibits a reverse behavior in response to fluid temperature and concentration. As a concequence, velocity boundary layer thickness hikes while thermal boundary layer thickness and concentration boundary layer thickness get diminution.

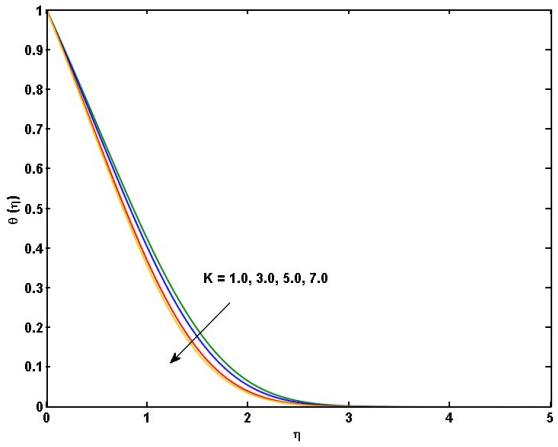

Fig. 15. Effect of K on $\theta(\eta)$ for $Z=\Lambda=0.2$, $D=0.2$, $p=1.5, We=3, B_1=0.5$, $N_b=N_t=0.2, \Pr=1.9$

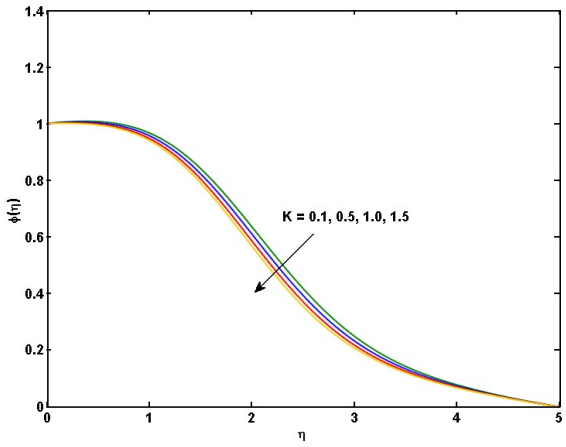

Fig. 16. Effect of p on $\phi(\eta)$ for $Z=\Lambda=0.2$, $We=3, B_1=0.5, D=0.2, p=1.5$, $N_b=N_t=0.2, \Pr=1.9, Sc=1$

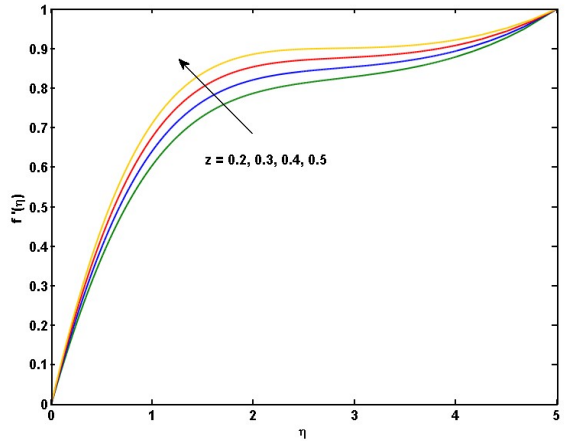

Fig. 17. Effect of Z on $f'(\eta)$ for $\Lambda=0.2$, $B_1=0.5, K=0.3, D=0.2, We=3, p=1.5$

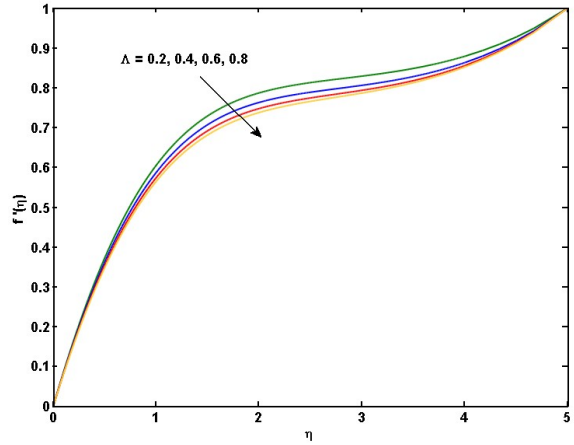

Fig. 18. Effect of Λ on $f'(\eta)$ for $Z=0.2$, $B_1=0.5, K=0.3, D=0.2, We=3, p=1.5$

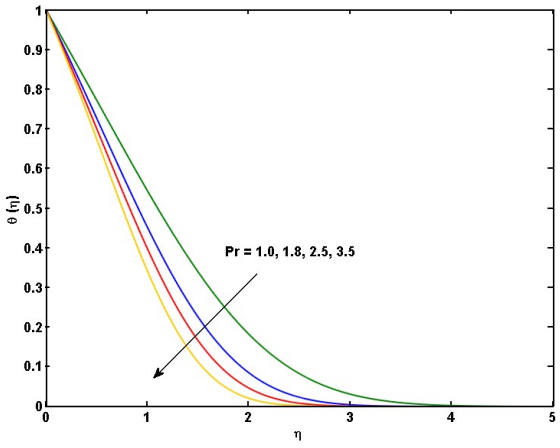

Fig. 19. Effect of Pr on $\theta(\eta)$ for $Z = \Lambda = 0.2$, $D = 0.2$, $p = 1.5, We = 3, B_1 = 0.5, K = 0.3$, $N_b = N_t = 0.2$

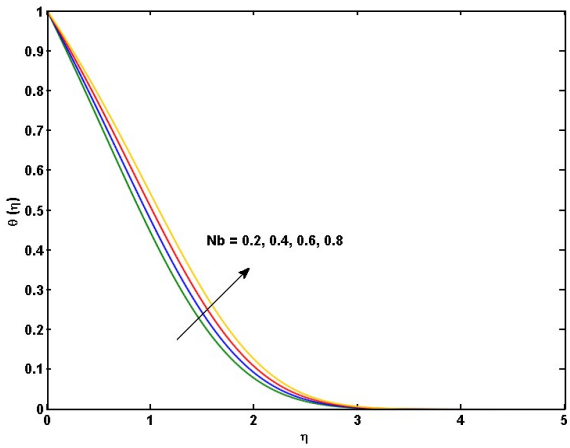

Fig. 20. Effect of N_b on $\theta(\eta)$ for $Z = \Lambda = 0.2$, $D = 0.2$, $p = 1.5, We = 3, B_1 = 0.5, K = 0.3$, $N_t = 0.2, \Pr = 1.9$

Figure 17 is viewed as an indication of the variation of velocity distribution under the impact of modified Hartmann number *Z*. Augmented Z leads to accelerated fluid motion, thereby establishing an ascending velocity boundary layer. The fundamental reason behind this fluid acceleration is that the flow over the plate is supported by surface parallel Lorentz force. In other words, an increase in magnetic field strength contributes to greater electromagnetic field. Thereby, narrowing the velocity boundary layer and enhancing the wall velocity gradient. From Fig. 18, it is understood that an increase in the angle of inclination contributes decelerated flow of shear-thickening fluid. High Prandtl fluids having low thermal diffusivity causes the decline of temperature leading to high heat transfer rate from the plate (Fig.19).

Intensive Brownian motion of particles (due to high bombardment of particles) upsurges the fluid temperature (Fig. 20) and undermines the fluid concentration (Fig. 21). Increasing N_t (due to high thermophoretic force) would amount to a significant increment in the fluid temperature as well as concentration (Figs. 22 and 23). This is because larger thermophoretic force drives more nanoparticles from the plate towards the ambient (Fig.23). As we move away and away from the plate, the absolute maximum of concentration curves rises up. As η increases the peaks of the concentration curves and shift towards right, indicates that nanoparticle concentration will upgrade gradually as we go farther and farther from the surface of the plate (Fig.23). Enhancing Sc uplifts the concentration along with some beautiful overshoots adjacent to the plate. Also, as Sc increases, the absolute maximum of the concentration curves contiguous to the plate enhances followed by an asymptotic decline of concentration in the flow domain (Fig. 24).

Figure 25 demonstrates the importance of B_1 and D on the variation of skin friction coefficient with We for shear-thickening fluid. An increase in D upgrades the wall shear-stress while that of B_1 undermines it. This is due to the fact that fluid velocity increases due to a rise in viscosity of the fluid. Figure 26 conveys the variation of skin friction coefficient against We for diferent values of *Z* and *p*. Increasing values of *Z* and *p* upsurge the wall shear-stress, but in a different fashion. The behavior of skin friction coefficient against We in response to different *K* and Λ is seen in Fig. 27. A rise in values in *K* enhances the wall shear-stress while that of Λ declines it (Fig. 27). Augmented B_1 ups the heat transfer rate from the plate while that of *D* reduces it (Fig. 28).

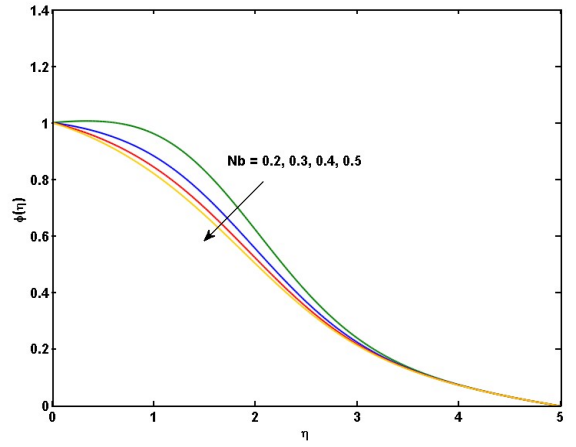

Fig. 21. Effect of N_b on $\phi(\eta)$ for $Z = \Lambda = 0.2$, $K = 0.3$, $We = 3, B_1 = 0.5, D = 0.2, p = 1.5$, $N_t = 0.2, \Pr = 1.9, Sc = 1$

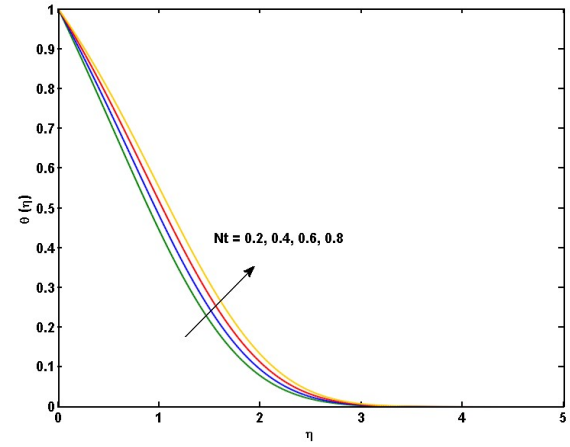

Fig. 22. Effect of N_t on $\theta(\eta)$ for $Z = \Lambda = 0.2$, $D = 0.2$, $p = 1.5, We = 3, B_1 = 0.5, K = 0.3$, $N_b = 0.2, \Pr = 1.9$

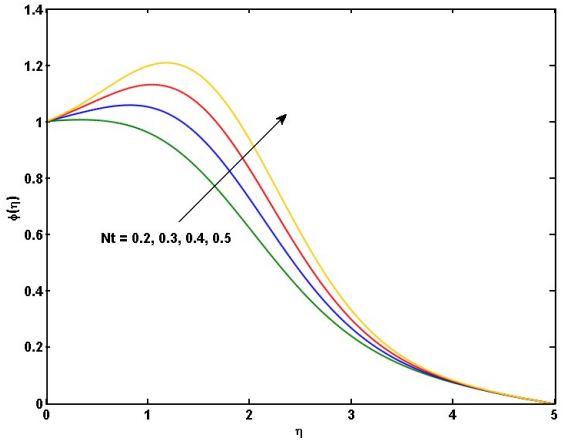

Fig. 23. Effect of N_t on $\phi(\eta)$ for $Z = \Lambda = 0.2$, $K = 0.3, We = 3, B_1 = 0.5, D = 0.2, p = 1.5, N_b = 0.2, \Pr = 1.9, Sc = 1$

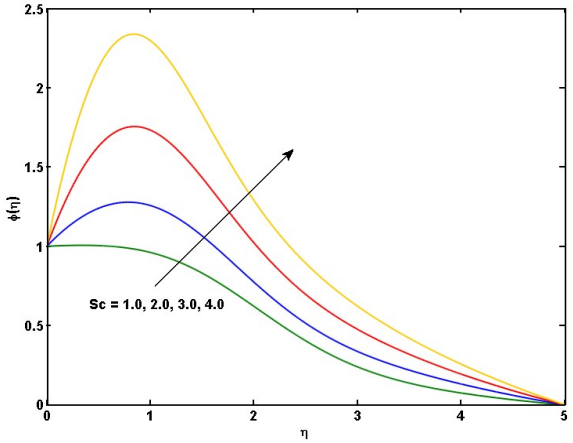

Fig. 24. Effect of Sc on $\phi(\eta)$ for $Z = \Lambda = 0.2$, $K = 0.3, We = 3, B_1 = 0.5, D = 0.2, p = 1.5, N_b = N_t = 0.2, \Pr = 1.9$

Further increment in N_b and N_t contributes the same behavior of Nusselt number in reducing the heat transfer rate (Fig. 29). This is because greater Brownian motion and thermophoretic force enhance the fluid temperature significantly. Figure 30 indicates the graphical representations of Sherwood Number against *Sc* for different B_1 and *D*. Increment in *D* uplifts wall mass transfer and that of B_1 vdeclines it for shear-thickening fluid. Wall mass transfer enhances due to an increase in N_b and that reduces with increase in N_t in response to different *Sc*.

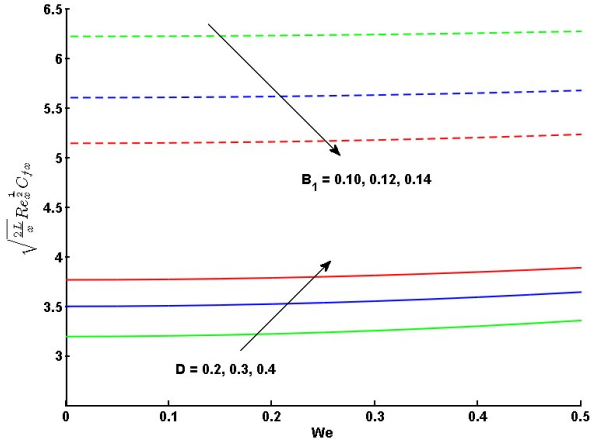

Fig. 25. Effects of D and B_1 on skin friction for $Z = \Lambda = 0.2$, $K = 0.3, We = 3, p = 1.5, N_b = N_t = 0.2, \Pr = 1.9$

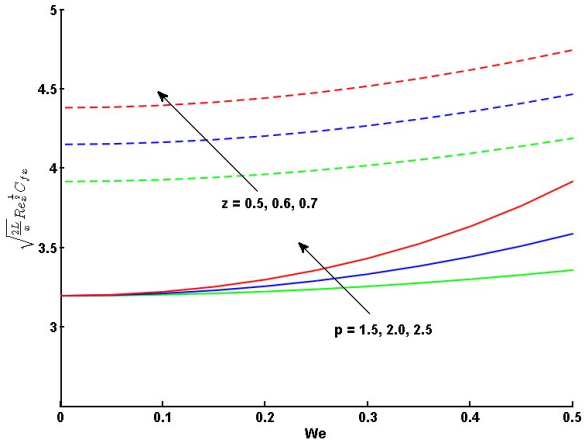

Fig. 26. Effects of Z and p on skin friction for $\Lambda = D = 0.2$, $K = 0.3, We = 3, B_1 = 0.5, N_b = N_t = 0.2, \Pr = 1.9$

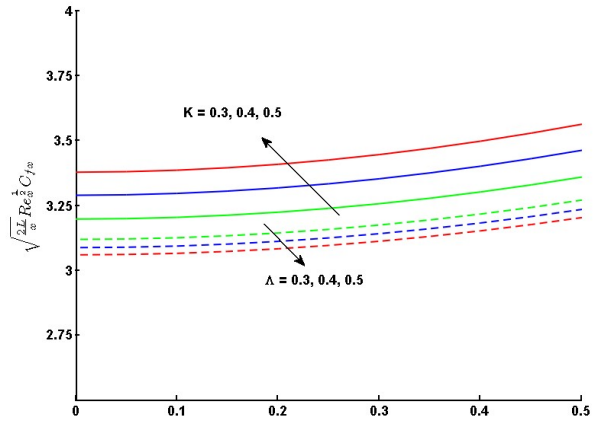

Fig. 27. Effects of K and Λ on skin friction $Z = D = 0.2$, $K = 0.3, We = 3, B_1 = 0.5, p = 1.5, N_b = N_t = 0.2, \Pr = 1.9$

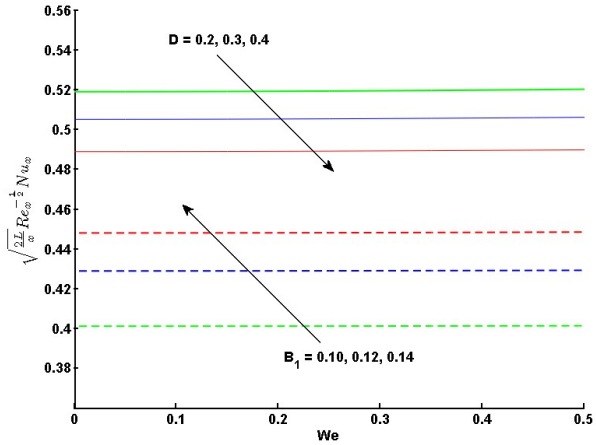

Fig. 28. Effects of D and B_1 on Nusselt number for $Z = \Lambda = D = 0.2$, $K = 0.3, We = 3, p = 0.2, N_b = N_t = 0.2, \Pr = 1.9$

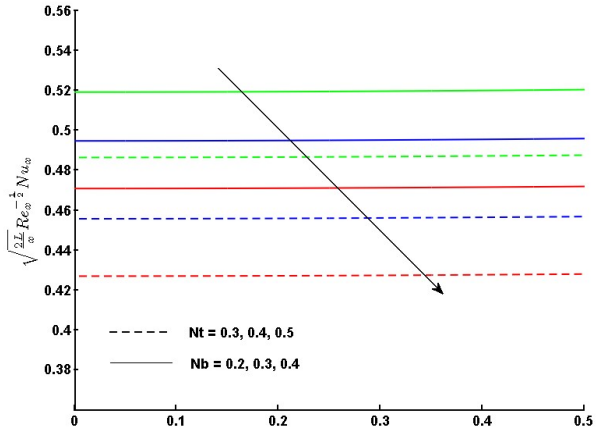

Fig. 29. Effects of N_t and N_b on Nusselt number for $Z = \Lambda = D = 0.2,\ K = 0.3, We = 3, p = 0.2, B_1 = 0.5,\ \Pr = 1.9$

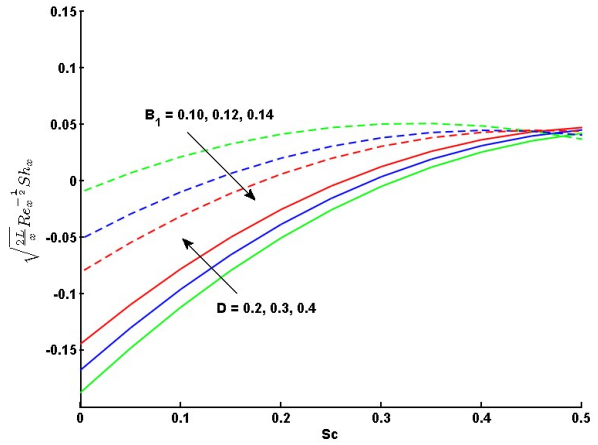

Fig. 30. Effects of D and B_1 on Sherwood number for $Z = \Lambda = 0.2,\ K = 0.3, We = 3, p = 1.5,\ N_t = N_b = 0.2, \Pr = 1.9$

4. Conclusion

The important outcomes of the present investigation are as follows:

- Enhancing D establishes thicker VBL and squeezes TBL as well as CBL while that of B_1 exhibits opposite trend.
- VBL is an increasing function of We while TBL and CBL are descending function of it.
- Significant accelerated motion is achieved for shear-thickening fluid compared to shear- thinning fluid.
- Augmentation in K hikes $f'(\eta)$ and belittles $\theta(\eta)$ and $\phi(\eta)$.
- An increase in the angle of inclination accounts for the retarded flow of shear-thickening fluid.
- Augmented Z establishes an ascending VBL in the flow domain.
- Higher Brownian motion and thermophoretic force yield more temperature and concentration leading to the reduction in HTR from the plate.

Conflict of Interest

The author(s) declared no potential conflicts of interest with respect to the research, authorship and publication of this article.

Funding

The author(s) received no financial support for the research, authorship and publication of this article.

Nomenclature

(u, v)	Velocity components in x and y directions $\left[m\,s^{-1}\right]$	η	Non-dimensional vertical distance
C	Nanoparticle concentration	C_∞	Ambient nanoparticle concentration
a	A constant $\left(s^{-1}\right)$	Z	Modified Hartmann number
$\theta(\eta)$	Non-dimensional temperature	$\phi(\eta)$	Non-dimensional concentration
υ_f	Kinematic viscosity $\left[m_2 s^{-1}\right]$	p	Power-law index
T	Fluid temperature $[K]$	$\tau_w(x)$	Wall shear stress $\left(kg\,m^{-1}s^{-2}\right)$
T_∞	Ambient fluid temperature $[K]$	We	Weissenberg number
N_b	Brownian motion parameter	N_t	Thermophoresis parameter
$\left(\rho C_p\right)_f$	Heat capacitance of base fluid $\left(J\,kg^2\,m^3K^{-1}\right)$	k_f	Thermal conductivity $\left[W.m^{-1}.K^{-1}\right]$
ρ_f	Density of base fluid $\left[kg\,m^{-1}\right]$	$\tau = \left(\rho C_p\right)_p / \left(\rho C_p\right)_f$	Heat capacity ratio
M_0	Magnetization $[T]$	δ	Width of magnets and electrodes $[m]$
D_T	Thermophoretic diffusion coefficient $\left[m^2 s^{-1}.k^{-1}\right]$	q_w	Wall heat flux $\left[W\ m^{-2}\right]$
D_B	Brownian diffusion coefficient $\left[m^2 s^{-1}\right]$	j_0	Current density $\left[A\,m^{-2}\right]$

P_r	Prandtl number	K	Porosity parameter
Λ	Width parameter	$f(\eta)$	Dimensionless stream function
VBL	Velocity boundary layer	HTR	Heat transfer rate
TBL	Thermal boundary layer	CBL	Concentration boundary layer
μ_f	Dynamic viscosity of base fluid $[Pa.s]$	L	Reference length $[m]$
Sc	Schmidt number	ρ_p	Density of nanoparticles $[kg\ m^{-1}]$
Subscripts			
f	Fluid	p	Particle
w	Quantities at wall	∞	Quantities at free stream

References

[1] S.U.S. Choi, Enhancing thermal conductivity of fluids with nanoparticles, *ASME Fluids Eng. Division* 231 (1995) 99–105.

[2] Y. Xuan, Q. Li, Investigation on convective heat transfer and flow features of nanofluids, *J. Heat Transfer* 125 (2003) 151-155.

[3] N. Kumar, S.S. Sonawane, Experimental study of Fe2O3/water and Fe2O3/ ethylene glycol nanofluid heat transfer enhancement in a shell and tube heat exchanger, *Int. Commun. Heat Mass Transf.* 78 (2016) 277–284.

[4] W. Khan and I. Pop, Boundary-layer flow of a nanofluid past a stretching sheet, *Int. J. Heat Mass Transf.* 53 (2010) 2477-2483.

[5] Kh. Hosseinzadeh, F. Afsharpanah, S. Zamani, M. Gholinia, D.D. Ganji, A numerical investigation on ethylene glycol-titanium dioxide nanofluid convective flow over a stretching sheet in presence of heat generation/absorption, *Case Studies Therm. Eng.* 12 (2018) 228–236.

[6] S.S. Ghadikolaei, Kh. Hosseinzadeh, D.D. Ganji, B. Jafari, Nonlinear thermal radiation effect on magneto Casson nanofluid flow with Joule heating effect over an inclined porous stretching sheet, *Case Studies Therm. Eng.* 12 (2018) 176-187.

[7] S.S. Ghadikolaei, Kh. Hosseinzadeh, D.D. Ganji, Analysis of unsteady MHD Eyring-Powell squeezing flow in stretching channel with considering thermal radiation and Joule heating effect using AGM , *Case Studies in Therm. Eng.* 10 (2017) 579-594.

[8] S.S. Ghadikolaei, M. Yassari, H. Sadeghi, Kh. Hosseinzadeh, D.D. Ganji, Investigation on thermophysical properties of Tio2–Cu/H2O hybrid nanofluid transport dependent on shape factor in MHD stagnation point flow, *Powder Technol.* 322 (2017) 428-438.

[9] A.S. Dogonchi, M.Hatami, Kh. Hosseinzadeh, G. Domairry, Non-spherical particles sedimentation in an incompressible Newtonian medium by Padé approximation, *Powder Technol.* 278 (2015) 248-256.

[10] M.K. Nayak, N.S. Akbar, V.S. Pandey, Z.H. Khan, D. Tripathi, MHD 3D free convective flow of nanofluid over an exponential stretching sheet with chemical reaction, *Adv. Powder Technol.* 28(9) (2017) 2159-2166.

[11] M.K. Nayak, N.S. Akbar, V.S. Pandey, Z.H. Khan, D. Tripathi, 3D free convective MHD flow of nanofluid over permeable linear stretching sheet with thermal radiation, *Powder Technol.* 315 (2017) 205-215.

[12] M.K. Nayak, MHD 3D flow and heat transfer analysis of nanofluid by shrinking surface inspired by thermal radiation and viscous dissipation, *Int. J. Mech. Sci.* 124 (2017) 185-193.

[13] M. Khan and M. Azam, Unsteady heat and mass transfer mechanisms in MHD Carreau nanofluid flow, *J. Mol. Liq.* 225 (2017) 554-562.

[14] M. Khan, M. Azam, A. Munir, Unsteady Falkner-Skan flow of MHD Carreau nanofluid past a static/moving wedge with convective surface condition, *J. Mol. Liq.* 230 (2017) 48-58.

[15] A. Pantokratoras, E. Magyari, MHD free-convection boundary-layer flow from a Riga-plate, *J. Eng. Math.* 64 (2009) 303-315.

[16] R. Ahmad, M. Mustafa, M. Turkyilmazoglu, Buoyancy effects on nanofluid flow past a convectively heated vertical Riga-plate: A numerical study, *Int. J. Heat Mass Transf.* 111 (2017) 827–835.

[17] M.K. Nayak, S. Shaw, O.D. Makinde, A.J. Chamkha, Effects of Homogenous–Heterogeneous reactions on radiative NaCl-CNP nanofluid flow past a convectively heated vertical Riga plate, *J. Nanofluids* 7(4) (2018) 1-10.

[18] R. Mehmood, M.K. Nayak, Noreen Sher Akber, O.D. Makinde, Effects of thermal-diffusion and diffusion-thermo on oblique stagnation point flow of couple stress Casson fluid over a stretched horizontal Riga plate with higher order chemical reaction, *J. Nanofluids* 8(1) (2019) 94-102

[19] S. Shaw, M.K. Nayak, O.D. Makinde, Transient rotational flow of radiative nanofluids over an impermeable Riga plate with variable properties, *Defect and Diffusion Forum* 387 (2018) 640-652.

[20] M.K. Nayak, A.K. Abdul Hakeem, O.D. Makinde, Influence of Catteneo-Christov Heat Flux Model on Mixed Convection Flow of Third Grade Nanofluid over an Inclined Stretched Riga Plate, *Defect and Diffusion Forum* 387 (2018) 121-134.

[21] M.K. Nayak, M.M Bhatti, O.D. Makinde,N.S. Akbar, Transient Magneto-Squeezing Flow of NaCl-CNP Nanofluid over a Sensor Surface Inspired by Temperature Dependent Viscosity, *Defect and Diffusion Forum* 387 (2018) 600-614.

[22] M.K. Nayak, S. Shaw, O.D. Makinde, A. J. Chamkha, Investigation of Partial Slip and Viscous Dissipation Effects on the Radiative Tangent Hyperbolic Nanofluid Flow Past a Vertical Permeable Riga Plate with Internal Heating: Bungiorno Model, *J. Nanofluids* 8(1) 2019. DOI:10.1166/jon.2019.1576.

[23] M. Roy, P. Biswal, S. Roy, T. Basak, Heat flow visualization during mixed convection within entrapped porous triangular cavities with moving horizontal walls via heatline analysis, *Int. J Heat Mass Transf.* 108 (2017) 468–489.

[24] T. Javed, Z. Mehmood, M.A. Siddiqui, I. Pop, Study of heat transfer in water-Cu nanofluid saturated porous medium through two entrapped trapezoidal cavities under theinfluence of magnetic field, *J. Mol. Liq.* 240 (2017) 402-411.
[25] M.K. Nayak, Chemical reaction effect on MHD viscoelastic fluid over a stretching sheet through porous medium, *Meccanica* 51 (2016) 1699-1711.
[26] S.S. Ghadikolaei, Kh. Hosseinzadeh, D.D. Ganji, M. Hatami, Fe_3O_4–$(CH2OH)_2$ nanofluid analysis in a porous medium under MHD radiative boundary layer and dusty fluid, *J. Mol. Liq.* 258 (2018) 172-185.
[27] A. Ahmad, S. Asghar, S. Afzal, Flow of nanofluid past a Riga-plate, *J. Magn. Magn. Mater.* 402 (2016) 44–48.
[28] M. Alizadeh, A.S. Dogonchi, D.D. Ganji, Micropolar nanofluid flow and heat transfer between penetrable walls in the presence of thermal radiation and magnetic field, *Case Studies in Therm. Eng.* 12 (2018) 319–332.
[29] A.S. Dogonchi, M. Alizadeh, D.D. Ganji, Investigation of MHD Go-water nanofluid flow and heat transfer in a porous channel in the presence of thermal radiation effect, *Adv. Powder Technol.* 28(7) (2017) 1815-1825.
[30] S.S. Ghadikolaei, Kh. Hosseinzadeh, D.D. Ganji, Investigation on three dimensional squeezing flow of mixture base fluid (ethylene glycol-water) suspended by hybrid nanoparticle (Fe3O4-Ag) dependent on shape factor, *J. Mol. Liq.* 262 (2018) 376-388.
[31] M. Hatami, M. Sheikholeslami, M. Hosseini, D.D. Ganji, Analytical investigation of MHD nanofluid flow in non-parallel walls, *J. Mol. Liq.* 194 (2014) 251-259.